Chinese Chemical Letters 35 (2024) 109802

Contents lists available at ScienceDirect

Chinese Chemical Letters

journal homepage: www.elsevier.com/locate/cclet

Molecular crowding electrolytes for stabilizing Zn metal anode in rechargeable aqueous batteries

Li Lin[a], Song-Lin Tian[a], Zhen-Yu Hu[a], Yu Zhang[a], Li-Min Chang[c], Jia-Jun Wang[c], Wan-Qiang Liu[a,*], Qing-Shuang Wang[b,*], Fang Wang[a,d,*]

[a] School of Materials Science and Engineering, Changchun University of Science and Technology, Changchun 130022, China
[b] School of Life Science and Technology, Changchun University of Science and Technology, Changchun 130022, China
[c] Key Laboratory of Preparation and Applications of Environmental Friendly Materials of the Ministry of Education, Jilin Normal University, Changchun 130103, China
[d] Zhongshan Institute of Changchun University of Science and Technology, Zhongshan 528437, China

ARTICLE INFO

Article history:
Received 16 February 2024
Revised 29 February 2024
Accepted 20 March 2024
Available online 22 March 2024

Keywords:
Zinc ion batteries
Anode
Electrolyte
Solid electrolyte interphase
Molecular crowding effect

ABSTRACT

A solid electrolyte interphase (SEI) with a robust mechanical property and a high ionic conductivity is imperative for high-performance zinc metal batteries. However, it is difficult to form such a SEI directly from an electrolyte. In this work, a molecular crowding effect is based on the introduction of $Zn(OTF)_2$ and $Zn(ClO_4)_2$ to 2 mol/L $ZnSO_4$ electrolytes. Simulations and experiments indicate that the $Zn(OTF)_2$ and $Zn(ClO_4)_2$ not only create a molecularly crowded electrolyte environment to promote the interaction of $Zn^{2+}$and OTF^-, but also participate in the reduction to construct a robust and high ionic-conductive SEI, thus promoting metal zinc deposition to the (002) crystal surface. With this molecular crowding electrolyte, a high current density of 1 mA/cm^2 can be obtained by assembling symmetric batteries with Zn as the anode for over 1000 h. And in a temperature environment of −10 °C, a current density of 1 mA/cm^2 can be obtained by assembling symmetric batteries with Zn for over 200 h. Zn//Bi_2S_3/VS_4@C cells achieve a CE rate of up to 99.81% over 1000 cycles. Hence, the utilization of a molecular crowding electrolyte is deemed a highly effective approach to fabricating a sophisticated SEI for a zinc anode.

Rechargeable zinc batteries with high energy density are in high demand in our daily lives, from portable electronics to electric vehicles. In recent years, zinc metal batteries (ZMB) have attracted much attention due to their high theoretical specific capacity (820 mAh/g) [1–5]. Intrinsically, aqueous electrolytes are safer, nonflammable, less expensive, less toxic, more conductive and demand simpler and less complicated battery manufacturing environments than their organic counterparts. However, these Zn dendrites grown from the Zn anode cause serious safety concerns and dramatically shorten the lifespan, thus limiting the practical applications of ZMBs [6–10]. Actually, most aqueous ZMBs undergo serious capacity fading and poor cycle life due to the challenging electrochemistry of the Zn metal anode. Some issues are related to the chemical corrosion of the Zn anode, the continuous generation of byproducts, and the poor reversibility of Zn plating/stripping that results in low coulombic efficiencies and non-uniform and uncontrolled dendrite growth, eventually shortening the battery lifespan. In addition to Zn dendrites, the inevitable hydrogen evolution reaction (HER) on the Zn anode in slightly acidic aqueous electrolytes not only restrains the utilization and reversibility of Zn anode but also aggravates the formation of dendrites [11–15]. Additionally, the increased polarization and higher nucleation overpotential cause poor Zn anode utilization and impart huge stress in the bulk of the cathode due to the sluggish Zn^{2+} diffusion kinetics.

Even though aqueous ZMBs have made progress in the last decades, they still suffer from several issues related to the Zn metallic anode that hinder their commercialization and industrialization for large-scale applications. Several efforts have been made to address these challenging issues, including modifications to separators, modifications to the Zn surface, including the construction of protective layers and the structure design of Zn anodes, and electrolyte modifications [16–20]. Among them, electrolyte modification, a straightforward approach, has become the most commonly used and promising route to improve the Zn anode, which is also highly desirable for industrial applications because of its simplicity [21–25]. All these issues are strongly influenced by the presence of numerous “free water” molecules in the bulk electrolyte. In order to stabilize the interface between zinc anodes and

* Corresponding authors.
E-mail addresses: wqliu1979@126.com (W.-Q. Liu), wangqingshuang@163.com (Q.-S. Wang), f-wang-ssi@foxmail.com (F. Wang).

https://doi.org/10.1016/j.cclet.2024.109802
1001-8417/

electrolytes, researchers have been trying to explore interface design strategies. One strategy involves constructing a thick, layered barrier between the zinc electrode and the liquid electrolyte, thereby shielding it from direct contact with the liquid electrolyte. Despite the functional effectiveness of this artificial protective layer, the multiple processing steps are not innocuous to the battery assembly process. In addition, controlling the Zn^{2+} solvation structure in the bulk electrolyte can build a strong solid electrolyte interface (SEI) to stabilize the Zn anode, especially when there are anions such as AGGs (aggregated ion pairs, one anion coordinated with two or more Zn^{2+}) in the solvation sheath. It has been reported that the AGG structure in the electrolyte facilitates the formation of mechanically robust and Zn^{2+} conductive SEI [26–30]. Therefore, electrolyte systems with a high AGG dominant solvation structure seem more promising for ZMBs.

Herein, the dendrite growth and hydrogen evolution of the zinc anode electrode were effectively inhibited by the strategy of $Zn(OTF)_2$ and $Zn(ClO_4)_2$ mixed molecularly crowded electrolytes. It is attributed to the introduction of $Zn(OTF)_2$ and $Zn(ClO_4)_2$, which facilitates the interaction between F^- and $ClO_4{}^{2-}$ to form the high ionic-conductive SEI layer containing ZnF_2. The solvation structure of Zn^{2+} that is fully hydrated is revealed, facilitating the transfer of interfacial charge. The highly stable and reversible Zn plating/stripping have been demonstrated in both Zn||Cu and Zn||Zn batteries. Due to the stabilization of both electrodes in the hybrid eutectic electrolyte, we report a high current density of 1 mA/cm^2 can be achieved by assembling Zn||Zn symmetric batteries for more than 1000 h. And in a temperature range of −10 °C, Zn||Zn symmetric batteries can achieve a current density of 1 mA/cm^2 for a duration exceeding 200 h. Zn//Bi_2S_3/VS_4@C cells exhibit a capacity retention of 100% over a period of 1000 cycles. Therefore, the use of a eutectic electrolyte is considered to be an efficient way to construct an advanced SEI for a zinc anode.

The key to achieving a high-performance zinc metal battery is to construct an advanced SEI, which not only stabilizes the Zn anode for a long-life span but also reduces the resistance of the interface for high Zn^{2+} kinetics. Since the SEI is closely related to the Zn^{2+} solvation environment, manipulating the interaction between ions and molecules in the electrolyte to form a rational Zn^{2+} solvated structure seems critical [31]. The traditional $ZnSO_4$ electrolyte will exhibit uneven deposition, and the resulting dendrites and byproducts will also trigger zinc corrosion and hydrogen evolution reaction. The interaction between $Zn(OTF)_2$ and $Zn(ClO_4)_2$ promotes the breakdown of F^-, leading to the formation of ZnF_2 containing SEI after the introduction of molecularly packed electrolytes. A uniform electric field direction will be produced by the smooth SEI layer, reducing hydrogen evolution reactions and encouraging the accumulation of metal zinc on the (002) crystal surface.

The effect of the molecularly crowded electrolyte on the solvation structure of the 2 mol/L $ZnSO_4$ electrolyte was studied by a series of relevant spectral, Molecular dynamics (MD) simulations, and Density functional theory (DFT) calculations. It is clear observed from Fig. 1a that with the introduction of the molecular-crowded electrolyte, the contact Angle between the electrolyte and the Zn metal surface decreases from 81.5° to 41.5° The hydrophilic functional groups of the densely packed electrolyte can aid in the uniform distribution of the electrolyte on the electrode surface. As shown in Fig. 1b, the Raman spectra of molecularly crowded electrolyte usually displays two peaks at 188 and 561 cm^{-1}, which are assigned to $ClO_4{}^-$ and the two peaks at 793 and 938 cm^{-1}, which are assigned to OTF^-, respectively. As concentration increases, the peak intensity becomes more apparent. The molecular interaction between the molecular crowding electrolyte and zinc sulfate was further investigated by Fourier transform infrared spectroscopy (FT−IR). As shown in Fig. 1c, the molecularly crowded electrolyte exhibits wide and strong O–H tensile vibrations between 3000 cm^{-1} and 3700 cm^{-1}, and all the O–H peaks become narrow and shift with the increasing concentration. The results showed that the molecularly crowded electrolyte contained only a small amount of free water, and the water activity decreased significantly. In the ^{1}H NMR spectra of the electrolyte (Fig. 1d), the molecularly crowded electrolyte shows a significant chemical shift at the H_2O peak. This indicates that the electron density of correlated ^{1}H decreases, leading to the strengthening of the hydrogen bond network in water [32].

The solvation structure within the molecularly crowding electrolytes was further investigated through molecular dynamics (MD) simulations, providing enhanced insights into the modified solvation structure (Fig. 1e). The results demonstrate that the three components of $SO_4{}^{2-}$, $ClO_4{}^-$ and OTF^- coordinate with Zn^{2+} ions and enter the primary solvation shell of Zn^{2+} ions, aligning with the findings obtained from FTIR and Raman spectroscopy. The composition of the inner solvation shell within the systems was precisely determined by analyzing the corresponding radial distribution functions (RDFs) and coordination results. In the molecular crowding electrolytes model, three distinct coordination peaks involving Zn−O from Zn−SO_4, Zn−OTF and Zn−ClO_4 are observed at ≈ 0.18 Å, confirming the participation of $SO_4{}^{2-}$, $ClO_4{}^-$ and OTF^- molecules in reconstructing the solvation shell (Fig. 1f). Additionally, the average coordination numbers of Zn−SO_4, Zn−OTF and Zn−ClO_4 are 2.8, 0.74, and 0.43, respectively (Fig. 1f). These simulation results indicate that the liquid eutectic solvation shell is formed through the intermolecular forces between $SO_4{}^{2-}$, $ClO_4{}^-$ and OTF^- molecules. Importantly, the addition of molecularly crowded electrolytes contributes to the reduction of free water activity. The adsorption Energy between the sulfonate of H_2O and Zn is calculated to be −2.05 eV by density functional theory (DFT) (Fig. 1g), which is much higher than those of Zn−OTF (−5.18 eV) and Zn−ClO_4 (−5.05 eV) interactions. This implies that a strong interaction between Zn and the $ClO_4{}^-$ and OTF^- molecules. Consequently, it is probable that the water molecules surrounding the molecularly crowded electrolyte possess distinct bonding networks in comparison to the bulk water environment.

In order to explain the influence of molecularly crowded electrolyte on zinc anode, the Electrochemical impedance spectroscopy (EIS) spectra of the ZMBs with different electrolytes were measured. As shown in Fig. S1 (Supporting information), it indicates that the charge transfer resistance of the Zn/Zn symmetric cell with molecular crowding electrolyte is smaller than the battery without the molecular crowding electrolyte. This is due to the interaction of molecule crowded electrolytes to produce a smooth SEI layer, which effectively reduces a zinc corrosion. Since chronoamperometry (CA) is a common technique capable of capturing changes in surface structure and the nucleation process, CA is additionally employed to investigate the genesis of the deposited film [33]. As shown in Fig. 2a, the current density of the bare Zn metal, continues to increase even after 100s at an overpotential of 100 mV. In contrast, the initial Zn nucleation and two-dimensional diffusion process on the Zn electrode with molecular crowding electrolyte lasts only about 100s and has a flat platform. This is closely related to the three-dimensional diffusion process, indicating that surface-absorbed Zn^{2+} appear to be directly reduced to Zn^0 as a result of strain-controlled two-dimensional surface diffusion. In addition, compared with bare zinc metal (−0.017 V), the potential of zinc symmetrical battery with molecular crowding electrolyte as a higher potential of −0.009 V, following with the weaker corrosion reaction tendency. Thus, the anticorrosion ability of molecular crowding electrolyte is due to the formation of a stable protective layer of $Zn(H_2O)_6{}^{2+}$ groups (Fig. 2b). Furthermore, the molecule-crowded electrolytes are also conducive to zinc deposition, thereby inhibiting zinc corrosion. Since Zn^{2+}−H_2O

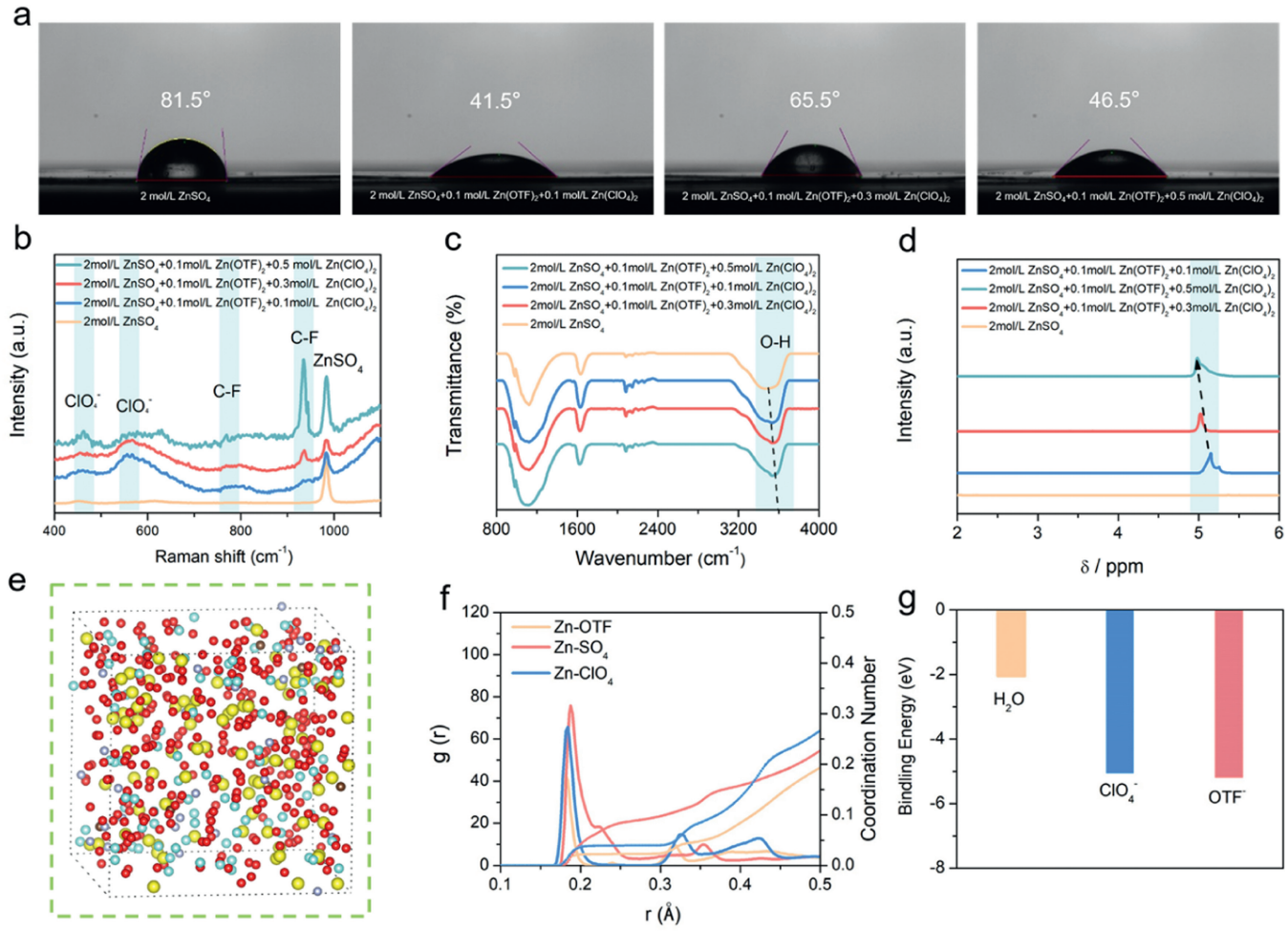

Fig. 1. (a) Contact angle of 2 mol/L $ZnSO_4$ on the Zn with different concentration of electrolytes. (b) Raman spectra of different concentration of electrolytes. (c) FTIR spectra of different concentration of electrolytes. (d) ^1H NMR spectra of different concentrations of the electrolytes. (e) 3D snapshot obtained by MD simulations of different concentration of electrolytes. (f) RDFs for Zn-O (H_2O), Zn-O (ClO_4^-), and Zn-O (OTF^-) collected from MD simulations in different concentration of electrolytes. (g) Binding energy of Zn^{2+} with H_2O, ClO_4^-, and OTF^- ion from DFT calculation.

is considered to be the culprit causing HER in the electrochemical process, we also used linear sweep voltammetry (LSV) to study the corrosion resistance of Zn with or without molecule-crowded electrolytes (Fig. 2c). Specifically, the inhibiting effect of molecule-crowded electrolytes on hydrogen evolution is shown by the significantly higher HER overpotential in cells of Zn containing molecule-crowded electrolytes than that of bare Zn. To confirm the benefits of molecular crowding effect on the Zn electrochemistry, Zn plating/stripping reaction was preliminarily investigated using cyclic voltammetry (CV). The CV curves of Zn||Cu asymmetric batteries with molecule-crowded electrolytes shows a weaker oxidation–reduction peak (Fig. S2 in Supporting information), further demonstrating the inhibition of hydrogen evolution reaction. Additionally, the Energy change is reflected in the larger nucleation overpotential ($ZnSO_4$ electrolyte: −0.17 V; 1.0% molecule crowded electrolyte: −0.18 V) (Fig. S3 in Supporting information). Larger nucleation overpotential is helpful for effectively controlling the rampant deposition process. The coulomb efficiency (CE) of the Zn||Cu coin-type battery with molecule-crowded electrolytes shows excellent electrochemical performance because it regulates the zinc plating/stripping process and inhibits corrosion by water. As shown in Fig. 2d, in contrast to the rapid battery failure observed on the bare Zn, the Zn electrode with molecule-crowded electrolytes demonstrated a high level of reversibility over 180 cycles with an average CE of 99.4%. Noticeably, the initial CE with molecule crowded electrolyte of 80.5% is much higher than that of without molecule crowded electrolyte (62.1%), substantiating the excellent side reaction inhibition capability of the molecule crowded electrolyte from the initial stage (Fig. S4 in Supporting information). The Zn symmetric battery, which is equipped with molecule-crowded electrolytes, exhibits exceptional cycle stability and a cycle life of more than 1000 h at a current density of 1 mA/cm^2, resulting in a capacity of 1 mAh/cm^2, which is nearly 10 times that of a battery without molecule-crowded electrolytes (Fig. 2e). And the Zn symmetric battery with molecule-crowded electrolytes cycled for more than 700 h at a current density of 4 mA/cm^2 with a capacity of 1 mAh/cm^2 (Fig. S5 in Supporting information). As the current density increases, Zn/Zn symmetric cells with molecule-crowded electrolytes also show excellent rate performance and lower overpotential across different current densities (Fig. 2f), which ensures adequate Zn^{2+} ions recruitment at high rates. Thus, even at −10 °C, Zn/Zn symmetric batteries with molecule-crowded electrolytes exhibit superior cycle stability over 200 h (Fig. 2g).

In order to verify the inhibitory effect of molecule-crowded electrolytes on dendrite growth, the zinc deposition behavior of bare Zn symmetrical batteries with and without molecule-crowded electrolytes was tracked by SEM characterization. When the current density is 4 mA/cm^2 and the capacity is 1 mAh/cm^2, the surface of the bare zinc anode exhibits a rough surface with some

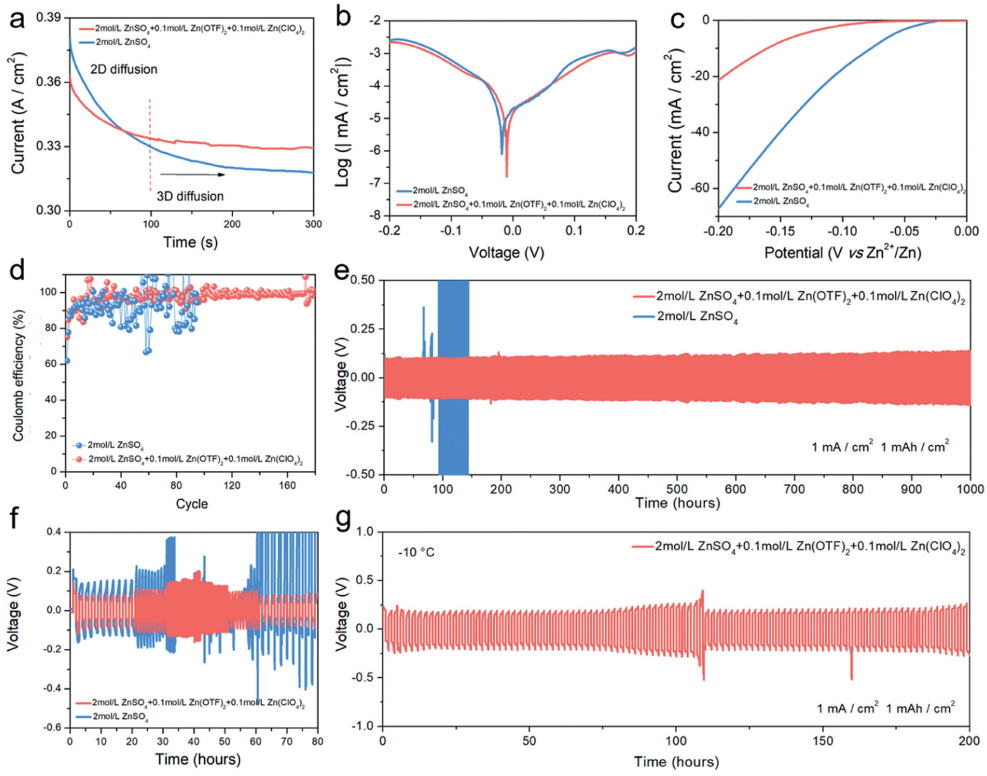

Fig. 2. (a) CA curves of bare Zn at an overpotential of 100 mV with 2 mol/L $ZnSO_4$ and 2 mol/L $ZnSO_4$ + 0.1 mol/L $Zn(OTF)_2$ + 0.1 mol/L $Zn(ClO_4)_2$ electrolytes. (b) Linear polarization curves showing the corrosion on bare Zn with 2 mol/L $ZnSO_4$ and 2 mol/L $ZnSO_4$ + 0.1 mol/L $Zn(OTF)_2$ + 0.1 mol/L $Zn(ClO_4)_2$ electrolytes. (c) Linear voltammetry curves showing the on bare Zn with 2 mol/L $ZnSO_4$ and 2 mol/L $ZnSO_4$ + 0.1 mol/L $Zn(OTF)_2$ + 0.1 mol/L $Zn(ClO_4)_2$ electrolytes. (d) Coulombic efficiency during cycling with 2 mol/L $ZnSO_4$ and 2 mol/L $ZnSO_4$ + 0.1 mol/L $Zn(OTF)_2$ + 0.1 mol/L $Zn(ClO_4)_2$ electrolytes. (e) Galvanostatic cycling of symmetrical cells at 1 mA/cm^2 and 1 mAh/cm^2 with 2 mol/L $ZnSO_4$ and 2 mol/L $ZnSO_4$ + 0.1 mol/L $Zn(OTF)_2$ + 0.1 mol/L $Zn(ClO_4)_2$ electrolytes. (f) Rate performance of Zn symmetric cell from 1 mA/cm^2 to 10 mA/cm^2 at an aerial capacity of 1 mAh/cm^2 with 2 mol/L $ZnSO_4$ and 2 mol/L $ZnSO_4$ + 0.1 mol/L $Zn(OTF)_2$ + 0.1 mol/L $Zn(ClO_4)_2$ electrolytes. (g) Galvanostatic cycling of symmetrical cells at 1 mA/cm^2 and 1 mAh/cm^2 with 2 mol/L $ZnSO_4$ and 2 mol/L $ZnSO_4$ + 0.1 mol/L $Zn(OTF)_2$ + 0.1 mol/L $Zn(ClO_4)_2$ electrolytes at −10 °C.

protrusions and zinc nanosheets (Figs. 3a and b). Alternatively, the zinc anode exhibiting molecule-crowded electrolytes exhibits a smooth and flat appearance (Figs. 3c and d), indicating the existence of a uniform and dense SEI layer on the zinc anode. This further indicates that the SEI layer can inhibit the growth of zinc dendrites [34]. However, the cross-sectional SEM image shows series dendrite growth on the exposed surface of the zinc anode. The morphological characterization and electrochemical results suggest that bare Zn with molecule-crowded electrolytes exhibits superior dendrite inhibition performance than Zn without molecule-crowded electrolytes, owing to its more uniform nucleation and lower nucleation overpotential. Therefore, XRD was used to further determine the deposition behavior of zinc with and without molecule-crowded electrolytes. As shown in Fig. 3e, compared with pure Zn metal without molecule-crowded electrolytes, the (002) crystal surface is obviously enhanced after 30 h cycling of Zn metal with molecule-crowded electrolytes, which proves the transformation of zinc deposition mode from (101) crystal plane to (002) crystal plane in a molecularly crowded electrolyte environment. In addition, Raman spectroscopy further demonstrated the inhibition effect of molecular crowded electrolyte on byproducts. As shown in Fig. 3f, compared with pure zinc metal with molecular crowded electrolyte, the Zn metal shows an obvious peak related to $Zn_4(OH)_6SO_4{\cdot}XH_2O$ (ZHS) at a Raman shift of about 988 cm^{-1} after being cycled for 30 h with zinc sulfate electrolyte, and the Zn metal shows no obvious peaks of zinc metal in the Raman spectra after being cycled with molecular crowded electrolyte for 30 h, demonstrating the excellent stability. And the chemical composition of the interfacial phase was further studied by XPS spectra. It can also be determined that the interface is mainly composed of ZnF_2 (Fig. 3g). Moreover, the growth of ZHS was inhibited (Fig. S6 in Supporting information). In order to prove the stability of Zn anode with molecular crowded electrolyte, we carried out an external experiment. In detail, we soaked pure zinc with and without molecular crowded electrolyte for 10 days, respectively (Fig. S7 in Supporting information). It was found that zinc anode surface produced similar protective layer, while the surface of zinc metal was seriously corroded by zinc sulfate. And the SEM images showed a more uniform stack of zinc sheets in the molecularly crowded electrolyte (Fig. S8 in Supporting information). Further, according to the XRD (Fig. S9 in Supporting information) and Raman (Fig. S10 in Supporting information) spectroscopy, the inhibition effect on ZHS-related byproduct can be proved, which further indicates that the molecular-crowded electrolyte promotes the formation of ZnF_2-containing layer, thus forming a stable SEI layer and inhibiting the growth of byproduct. DFT calculations were carried out for the adsorption behaviors of Zn^{2+}, ClO_4^-, and OTF^- on different Zn crystal planes (Fig. 3h). As elucidated, the adsorption energies of Zn^{2+}, ClO_4^-, and OTF^- on different Zn planes are −0.81 eV, −4.65 eV and −4.87 eV on (101) crystal plane, which are all significantly lower than those of Zn^{2+}, ClO_4^-, OTF^- on (002) crystal plane (−0.47, −3.21, and −3.31 eV), respectively. Therefore, the introduction of a molecularly crowded electrolyte preferentially adsorbed on the (101) zinc surface and deposited on the (002) crystal plane. In addition, XRD and SEM results further confirm that Zn^{2+} ions are more likely to be deposited into nucleation on the (002) crystal plane than on the (101) crystal planes.

The monitoring results by differential electrochemical mass spectrometry (DEMS) show almost no hydrogen evolution of the Zn/Zn symmetric battery with molecularly crowded electrolyte,

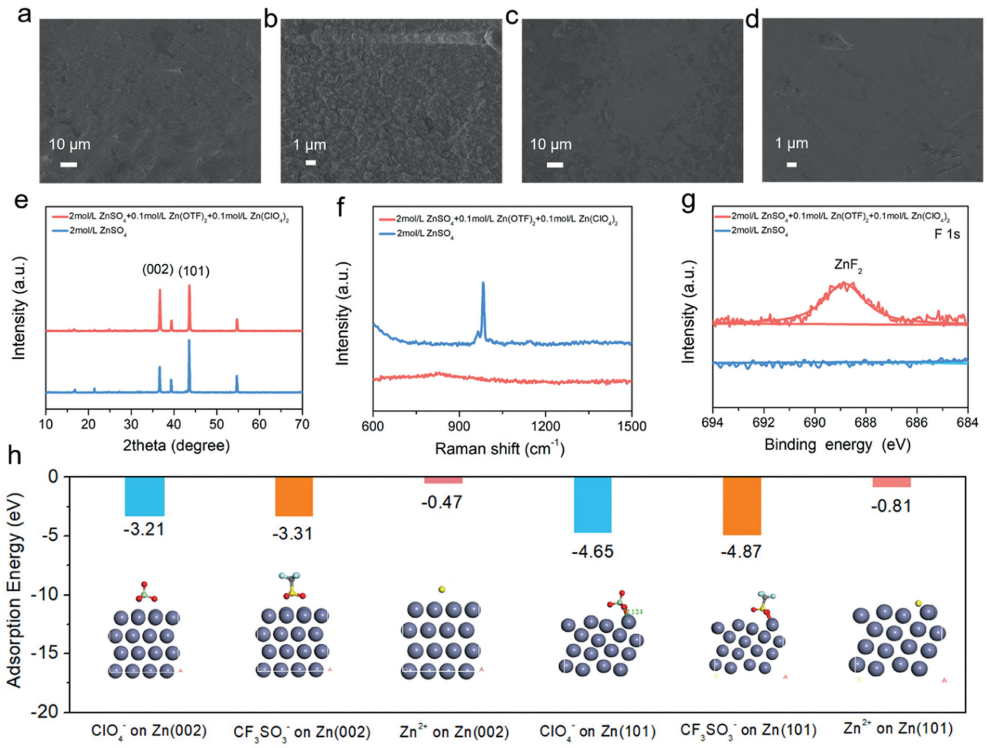

Fig. 3. (a, b) SEM images of bare Zn anode with 2 mol/L $ZnSO_4$ electrolyte after Zn plating for 4 mAh/cm^2 with a capacity of 1 mA/cm^2. (c, d) SEM images of bare Zn anode with 2 mol/L $ZnSO_4$ + 0.1 mol/L $Zn(OTF)_2$ + 0.1 mol/L $Zn(ClO_4)_2$ electrolyte after Zn plating for 4 mAh/cm^2 with a capacity of 1 mA/cm^2. (e) XRD patterns of bare Zn anode with 2 mol/L $ZnSO_4$ and 2 mol/L $ZnSO_4$ + 0.1 mol/L $Zn(OTF)_2$ + 0.1 mol/L $Zn(ClO_4)_2$ electrolytes after Zn plating for 4 mAh/cm^2 with a capacity of 1 mA/cm^2 for 30 h. (f) Raman patterns of bare Zn anode with 2 mol/L $ZnSO_4$ and 2 mol/L $ZnSO_4$ + 0.1 mol/L $Zn(OTF)_2$ + 0.1 mol/L $Zn(ClO_4)_2$ electrolytes after Zn plating for 4 mAh/cm^2 with a capacity of 1 mA/cm^2 for 30 h. (g) XPS spectra of F 1s for bare Zn anode with 2 mol/L $ZnSO_4$ and 2 mol/L $ZnSO_4$ + 0.1 mol/L $Zn(OTF)_2$ + 0.1 mol/L $Zn(ClO_4)_2$ electrolytes after Zn plating for 4 mAh/cm^2 with a capacity of 1 mA/cm^2 for 30 h. (h) Absorption Energy comparison of Zn^{2+}, ClO_4^- and OTF^- on various Zn crystal planes.

while the hydrogen evolution of the Zn symmetric battery increases gradually without molecularly crowded electrolyte, which further explains the effectively inhibition of a molecularly crowded electrolyte on hydrogen evolution (Fig. 4a). Furthermore, to verify the crowded effect on the Zn anode, *in situ* Raman spectroscopy is employed to investigate the transformation of Zn ions at the electrode/electrolyte interface within plating progress, where the Raman signal at 980 cm^{-1} corresponding to SO_4^{2-} is linked to the concentration fluctuations of Zn^{2+}. As shown in Fig. 4b, the Raman signal at 980 cm^{-1} shows a gradual decrease in strength during Zn deposition with molecularly crowded electrolyte, indicating a uniform distribution of Zn ions and inhibition of the formation of by-products. On the contrary, when *in situ* monitoring the region of interface between molecularly crowded electrolyte and Zn anode, the Raman signal intensity gradually strengthens (Fig. 4c), which can be attributed to uneven Zn ion distribution. The results of *in situ* Raman spectroscopy certify that the molecularly crowded electrolyte could regulate the distribution of the Zn ions to achieve uniform Zn deposition, which laid the foundation for dendrite-free Zn anode [35]. In addition to hydrogen evolution reaction, zinc anodes are often plagued by dendrite growth and zinc metal corrosion, primarily attributed to the uneven contact between the electrolyte and the surface of the zinc anode. In order to visually observe the effect of molecularly crowded electrolyte on zinc plating/stripping, Zn deposition behavior at a current density of 5 mA/cm^2 was monitored by *in-situ* optical microscopy. Obviously, zinc deposition on the exposed zinc metal was uneven, and dendrites appeared on the surface after only 10 min of cell operation (Fig. 4d). When the deposition time is 30 min, dendrites are produced gradually in the cross-section direction. In contrast, the Zn anode containing a molecularly crowded electrolyte exhibited uniform deposition behavior throughout the plating process, without any visible Zn dendrites being detected (Fig. 4e). This further indicates the inhibitory effect of molecular crowded electrolyte on zinc dendrites. This further demonstrates the inhibitory effect of electrolytes that are molecularly crowded on zinc dendrites. Based

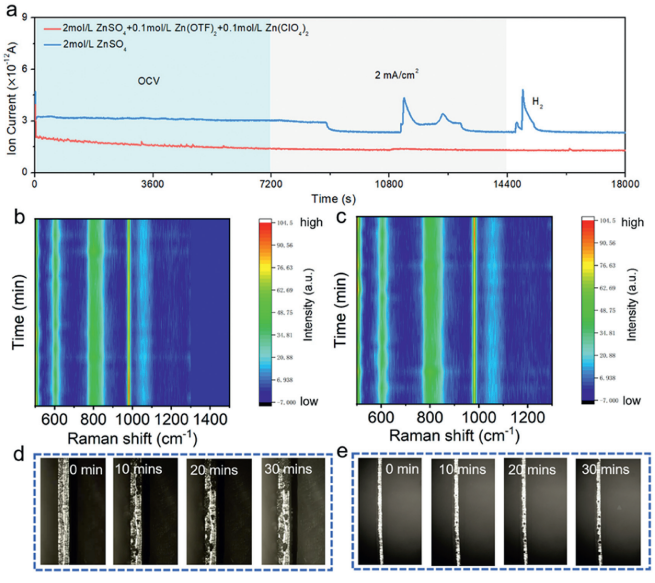

Fig. 4. (a) DEMS results of the discharged Zn symmetrical cells with 2 mol/L $ZnSO_4$ and 2 mol/L $ZnSO_4$ + 0.1 mol/L $Zn(OTF)_2$ + 0.1 mol/L $Zn(ClO_4)_2$ electrolytes at a current density of 2 mA/cm^2. (b, c) *In situ* Raman results of Zn||Zn with 2 mol/L $ZnSO_4$ and 2 mol/L $ZnSO_4$ + 0.1 mol/L $Zn(OTF)_2$ + 0.1 mol/L $Zn(ClO_4)_2$ electrolytes at initial cycle. (d, e) *In situ* optical visualization of Zn plating behavior of bare Zn and Zn@SbF_3 at 10 mA/cm^2 with 2 mol/L $ZnSO_4$ and 2 mol/L $ZnSO_4$ + 0.1 mol/L $Zn(OTF)_2$ + 0.1 mol/L $Zn(ClO_4)_2$ electrolytes.

on the above advanced *in situ* characterization, it was verified that the molecular crowding effect of the crowded electrolyte promoted the decomposition of OTF^-, thus forming the SEI layer containing ZnF_2, which not only inhibited the formation of by-products, but also inhibited the hydrogen evolution and corrosion of the zinc anode.

We further investigated the electrochemical properties of the full battery with a Zn anode and a Bi_2S_3/VS_4@C cathode. Fig. S11 (Supporting information) shows the SEM images of Bi_2S_3/VS_4@C, is a nanorod structure with an average length of about $\approx$ 5 μm. The elemental mapping of Fig. S12 (Supporting information) shows that Bi, V, S and C elements are uniformly distributed on the Bi_2S_3/VS_4@C cathode. The existence of Bi, V, S and C elements can also be proved by the Energy spectrum of the Bi_2S_3/VS_4@C cathode (Fig. S13 in Supporting information). The TEM image of the Bi_2S_3/VS_4@C cathode is shown in Fig. S14 (Supporting information). The coating of the carbon layer is clearly visible. The XRD analysis of the cathode of Bi_2S_3/VS_4@C cathode shows that the characteristic peaks of Bi_2S_3 and VS_4 are well matched with the Bi_2S_3/VS_4@C in Fig. S15 (Supporting information) indicating the successful synthesized composite of Bi_2S_3/VS_4@C. Further, the increased Raman peaks located at 171, 353 and 814 cm^{-1} prove the successful introduction of Bi_2S_3/VS_4@C (Fig. S16 in Supporting information). Fig. S17 (Supporting information) show that the XPS spectra revealed the presence of Bi 2p, S 2p, V 2p and C 1s in the cathode of Bi_2S_3/VS_4@C, without other impurities, indicating that the synthesis of Bi_2S_3/VS_4@C was successful. Furthermore, it confirms the existence of Bi_2S_3 and VS_4. The galvanostatic intermittent titration technique (GITT) test was then implemented to detect the Zn^{2+} diffusion behavior of the Zn//Bi_2S_3/VS_4@C battery with and without molecularly crowded electrolyte. As shown in Fig. S18 (Supporting information), the Zn^{2+} ion diffusion coefficient of the battery with molecularly crowded electrolyte is calculated to range about $10^{-11.8}$ cm^2/s, which is higher and more stable than that of the battery without molecularly crowded electrolyte, which ranges about $10^{-12.9}$ cm^2/s (Fig. S19 in Supporting information), revealing fast and stable migration kinetics for Zn^{2+} ions in molecularly crowded electrolyte. We performed EIS analysis and observed the morphological evolution of the Zn anode. The initial charge transfer resistance (R_{ct}) of a Zn//Bi_2S_3/VS_4@C battery with a molecularly crowded electrolyte is much smaller than that of a Zn//Bi_2S_3/VS_4@C battery. This indicates that the Zn anode with a molecularly crowded electrolyte exhibits the best zinc ion diffusion and charge transfer kinetics (Fig. S20 in Supporting information). Similar peaks in the CV curve indicate that the oxidation–reduction processes were the same with or without the molecularly crowded electrolyte (Fig. S21 in Supporting information). CV tests were used to validate this hypothesis on Bi_2S_3/VS_4@C at different scan rates ranged from 0.1 mV/s to 5 mV/s. As the scan rate increases, the peak value of CV gradually widens yet retains the initial curve's shape (Fig. S22a in Supporting information). Based on the relationship between the scanning rate and the peak current, the behavior of Zn ions in the Bi_2S_3/VS_4@C cathode was further studied to understand the storage mechanism of the electrode. The terms "scanning current density" and "scan rate" are utilized, respectively. As shown in Fig. S22b (Supporting information), we calculated the b values for the two redox peaks and found that they were 0.58 and 0.65, respectively. This suggests that both diffusion and capacitance mechanisms influence the charge storage in Bi_2S_3/VS_4@C. As depicted in Fig. S22c (Supporting information), it can be observed that at a scanning rate of 5 mV/s, the permittivity is maintained, and 89.67% accounts for the total capacity. And as the scanning rate increases, the amount of capacitance increases as well. (Fig. S22d in Supporting information). It is significant that this diffusion contribution is lower than the capacitance contribution. The electrochemical process exhibits a pseudocapacitive behavior at high scanning rates, which contributes to the attainment of high-velocity properties, allowing the diffusion process to exercise greater control over charge accumulation. The Zn//Bi_2S_3/VS_4@C battery with a molecularly crowded electrolyte exhibits a higher specific capacity of 614.4 mAh/g at a current density of 0.1 A/g compared with the bare Zn//Bi_2S_3/VS_4@C battery (482.4 mAh/g) (Fig. S23 in Supporting information). What is more, when the current density is increased to 1 A/g, the high specific capacity of 81 mAh/g can be obtained, which is much better than the bare Zn//Bi_2S_3/VS_4@C battery without a molecularly crowded electrolyte (56 mAh/g) under the normal conditions (Fig. S24 in Supporting information). Figs. S25 and S26 (Supporting information) demonstrate the charge and discharge performances of Zn//Bi_2S_3/VS_4@C batteries with and without the molecular crowded electrolytes at different current densities. As expected, Zn//Bi_2S_3/VS_4@C batteries with molecularly crowded electrolytes exhibit a long service cycle life at a current density 1 A/g, with a capacity retention rate of 94.8% and a CE rate of up to 99.81% after 1000 cycles (Fig. S27 in Supporting information). In contrast, the capacity of the bare Zn//Bi_2S_3/VS_4@C battery without the molecularly crowded electrolyte has a capacity retention rate of 12% after 1000 cycles. In detail, the rate performance and cycle stability of rechargeable batteries are often determined by dynamic processes.

In summary, the molecularly crowded electrolyte has the ability to effectively promote OTF^- decomposition and the interaction between Zn^{2+} and F^-, resulting in the formation of the SEI layer containing ZnF_2, which can effectively enhance the uniform deposition of Zn ions and improve the stability of the solid electrolyte/anode interface. Simultaneously, the interfacial coating has the capability to form a uniform Zn-rich layer on the Zn surface, accelerate the transfer of Zn^{2+} ions, limit the coarse two-dimensional diffusion, ultimately result in uniform and dense Zn deposition. In addition, it is found that the introduction of molecular crowded electrolyte can regulate the deposition process of Zn to (002) crystal surface via the MD simulation and DFT calculation. The results show that the modified zinc anode with molecularly crowded electrolytes can run stably for more than 1000 h, and it can also maintain a stable cycle in a low temperature environment of −10 °C. The average coulomb efficiency of the whole battery composed of Bi_2S_3/VS_4@C cathode can reach 94.8% and a CE rate of up to 99.81% after 1000 cycles. This work not only analyzes the impact of molecular crowding on zinc anodes but also proposes a highly efficient operational solution for the development of zinc anodes with a long lifespan, low cost and high safety.

Declaration of competing interests

The authors declare that they have no known competing financial interests or personal relationships that could have appeared to influence the work reported in this paper.

Acknowledgments

This research was supported by Jilin Provincial Natural Fund (No. 20230101205JC), Chongqing Natural Science Foundation (Nos. cstc2022jcyj-msxmX0184 and CSTB2022NSCQ-MSX0241), the International Cooperation Foundation (No. 20220402026GH) of Science and Technology Department of Jilin Province.

Supplementary materials

Supplementary material associated with this article can be found, in the online version, at doi:10.1016/j.cclet.2024.109802.

References

[1] J.X. Zheng, Q. Zhao, T. Tang, et al., Science 366 (2019) 645–648.
[2] L. Lin, S.L. Tian, L. Fang, et al., J. Ener. Stor. 72 (2023) 108356.
[3] L. Lin, S.L. Tian, L.M. Chang, et al., Alloys Compd. 985 (2024) 174049.
[4] N. Zhao, Y. Liang, W. Huo, et al., Chin. Chem. Lett. (2023) 109332.
[5] W. Wu, Y. Deng, G. Chen, et al., Chin. Chem. Lett. 34 (2023) 108424.
[6] H. Tian, J. Yang, Y. Deng, et al., Adv. Ener. Mater. 13 (2022) 2202603.
[7] Y. Xia, R. Tong, J. Zhang, et al., Nano-Micro Lett. 16 (2024) 96.
[8] Y. Chen, Z. Deng, Y. Sun, et al., Nano-Micro Lett. 16 (2024) 82.
[9] Z. Zhu, Z. Lin, Z. Sun, et al., Rare Metals 41 (2022) 3729–3739.
[10] J. Wan, R. Wang, Z. Liu, et al., Adv. Mater. 36 (2024) 2310623.
[11] T. Wang, Y. Tang, M. Yu, et al., Adv. Funct. Mater. 33 (2023) 2306101.
[12] Y. Cheng, Y. Jiao, P. Wu, Ener. Environ. Sci. 16 (2023) 4561–4571.
[13] X. Song, L. Bai, C. Wang, et al., ACS Nano 17 (2023) 15113–15124.
[14] M. Qiu, P. Sun, G. Cui, W. Mai, ACS Appl. Mater. Interfaces 14 (2022) 40951–40958.
[15] C. Li, Q. Shao, K. Luo, et al., Adv. Funct. Mater. 33 (2023) 2305204.
[16] L. Han, Y. Guo, F. Ning, et al., Adv. Mater. 36 (2024) 2308086.
[17] Y. Du, Y. Feng, R. Li, et al., Small (2023), doi:10.1002/smll.202307848.
[18] D. Li, Y. Tang, S. Liang, et al., Ener. Environ. Sci. 16 (2023) 3381–3390.
[19] J. Cao, Y. Sun, D. Zhang, et al., Adv. Ener. Mater. 14 (2024) 2302770.
[20] C. Chang, S. Hu, T. Li, et al., Ener. Environ. Sci. 17 (2024) 680–694.
[21] Y. Hu, Z. Wang, Y. Li, et al., Chem. Eng. J. 479 (2024) 147762.
[22] T. Zhang, J. Yang, H. Wang, et al., Ener. Stor. Mater. 65 (2024) 103085.
[23] D. Qiu, B. Li, C. Zhao, et al., Ener. Stor. Mater. 61 (2023) 102903.
[24] Z. Zha, T. Sun, D. Li, et al., Ener. Stor. Mater. 64 (2024) 103059.
[25] L. Lin, S. Tian, L. Chang, et al., J. Alloys Compd. 985 (2024) 174049.
[26] Y. Yu, P. Zhang, W. Wang, J. Liu, Small Methods 7 (2023) 2300546.
[27] Y. Wu, T. Zhang, L. Chen, et al., Adv. Ener. Mater. 13 (2023) 2300719.
[28] D. Feng, Y. Jiao, P. Wu, Angew. Chem. Int. Ed. 62 (2023) 202314456.
[29] R. Wang, Q. Ma, L. Zhang, et al., Adv. Ener. Mater. 13 (2023) 2302543.
[30] H. Peng, X. Wang, F. Yang, et al., Chem. Eng. J. 474 (2023) 145864.
[31] H. Tu, L. Li, Z. Wang, et al., ACS Nano 16 (2022) 16898–16908.
[32] M. Wu, X. Wang, F. Zhang, et al., Ener. Environ. Sci. 17 (2023) 619–629.
[33] M. Fu, Q. Zhao, K. Long, et al., Adv. Funct. Mater. 34 (2024) 2311680.
[34] S. Wu, J. Chen, Z. Su, et al., Small 18 (2022) 2202992.
[35] Z. Lv, Y. Kang, G. Chen, et al., Adv. Funct. Mater. 34 (2024) 2310476.